Contrasting atmospheric and climate dynamics of the last-glacial and Holocene periods

Peter D. Ditlevsen*, Henrik Svensmark† & Sigfus Johnsen*‡

* The Niels Bohr Institute, Department for Geophysics, University of Copenhagen, Juliane Maries Vej 30, DK-2100 Copenhagen Ø, Denmark
† Solar-Terrestrial Physics Division, Danish Meteorological Institute, Lyngbyvej 100, DK-2100 Copenhagen Ø, Denmark
‡ Science Institute, Department of Geophysics, University of Iceland, Dunhaga 3, IS-107, Reykjavik, Iceland

Our present climate is relatively stable compared to that of the Last Glacial Maximum about 20,000 years ago. Palaeoclimate records obtained from ice cores[1,2] and deep-sea sediment cores[3] for the last glacial period show abrupt temperature changes on timescales of a few hundred years, which have been attributed to cycles of ice build-up and release associated with large ice sheets (Dansgaard–Oeschger cycles and Heinrich events)[3] and their coupling to ocean circulation[4,5]. But little is known about the dynamics of the atmosphere during the last glaciation. Ice sheets influence atmospheric circulation, and studies using general circulation models have suggested stormier, more variable atmospheric dynamics during the Last Glacial Maximum than today[6–9]. Here we report the results of an analysis of temporal trends over the past 91,000 years in the oxygen isotope signatures of a high-resolution ice-core record from Greenland[1,2]. This analysis provides direct evidence that atmospheric circulation during the last glaciation was more turbulent than it is today.

Climate dynamics are characterized by a variety of physical processes covering a large range of timescales. To retrieve information on the important physical processes it is crucial to obtain and analyse climate signals covering these timescales. The $\delta^{18}O$ isotope data extracted from the ice core provide, owing to the high snow accumulation rate in central Greenland, a high-resolution climate signal as a proxy for the temperature (see Fig. 1 legend).

The ice-core data analysed here covers the Holocene and last-glacial periods with a temporal resolution ranging from seasons in the present to ~10 yr at 91 kyr before present, BP (17,496 data points). The data is based on sampling slices of specified increments down through the ice core. The connection between the depth in the core and the age is established by counting of annual layers down to 14 kyr BP and a model for the ice-flow dynamics further down[10]. The full signal is shown in Fig. 1*a*. The power density spectrum is shown in Fig. 2.

There are two regimes of behaviour in the power spectrum separated at around a few hundred years. For timescales longer than 100–200 yr the spectrum is continuous, without dominant peaks, of the form $1/f^{\alpha}$ with $\alpha \approx 1.6$. At this point the spectral slope (~ -1.6) of the low-frequency part of the signal diminishes to ~1 (white noise). To separate the climate information of these two regimes we split the signal into a high- and a low-frequency part using a spectral cut at 150 years; Fig. 1*b* shows the 150-yr low-pass, and Fig. 1*c* is the 150-yr high-pass. To this we have applied a 20-yr low-pass to remove artificial trends in the record caused by a poorer resolution in the bottom of the record.

The characteristic "saw-tooth" variations of the low-pass filtered signal, of typical timescales around a few thousand years, have previously been assigned to the ice/ocean dynamics through ice-surges (Dansgaard–Oeschger and Heinrich events)[3]. The climate dynamics of these events are probably related to surging and build-up of the ice-caps, and coupling to the ocean circulation[4,5]. The surging is a very rapid process whereas the build-up takes more than a few hundred years, as the ice has to be transported as precipitation through the atmosphere. This could explain the saw-tooth shapes, which are maintained in the low-pass signal, Fig. 1*b*. There is at present no full understanding of the connection between the complex dynamics underlying the signal and the spectral characteristics. But the slope (−1.6) of the power spectrum indicates non-trivial dynamics over long timescales, in the sense that the signal cannot be explained as a simple autoregressive process. In a simple autoregressive process, as that of a stochastic climate model[11], the signal is generated by accumulation of independent identically distributed noise, representing the fast components of the climate system. The power spectrum will, for such a process, on timescales shorter than the correlation time always have a spectral slope of −2.

The residual high-pass signal (Fig. 1*c*) represents timescales faster than a few hundred years. This part of the signal contains the information on the atmospheric dynamics. The most striking feature of this signal is that the envelope of the fluctuations is roughly proportional to the degree of glaciation—or the tempera-

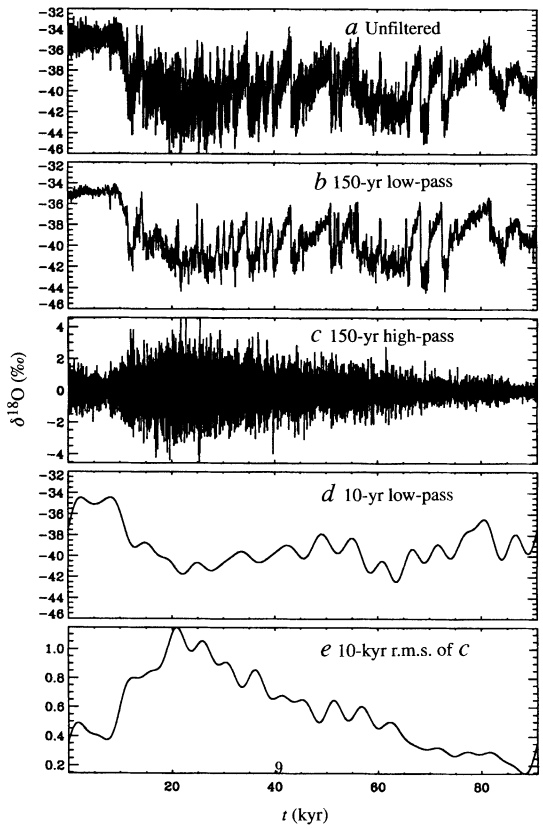

FIG. 1 *a*, The high-resolution $\delta^{18}O$ signal from the Greenland ice-cap. $\delta^{18}O$ is given (in units of ‰) by $[(^{18}O/^{16}O)_{ice}/(^{18}O/^{16}O)_{standard}] - 1$, where the standard is present-day ocean water. Empirically it has been shown that there is approximately a constant linear relationship between $\delta^{18}O$ in precipitation and the air temperature where the precipitation occurs[19]. The ice-cap thus constitutes a record which is a proxy for air temperature. The exact relationship between temperature and isotope ratio depends in an intricate way on the sea/air temperature of evaporation, cloud temperature of condensation, and the path followed by the vapour before falling out as snowflakes. Furthermore, the isotope ratio in the ice depends on molecular diffusion and mixing in the ice. The ice-core $\delta^{18}O$ ratio is therefore a proxy for some spatially and temporally averaged temperature signal, conditioned by a precipitation event. But we expect that these processes act as independent noise on the climate temperature signal contained in the record. *b*, The 150-yr low-pass of the $\delta^{18}O$ signal; *c*, the corresponding 150-yr high-pass. *d*, The 10-kyr low-pass of the $\delta^{18}O$ signal; and *e*, the 10-kyr low-pass of the absolute value of the 150-yr high-pass (c), corresponding to the 10-kyr root mean square (r.m.s.) of the high-pass.

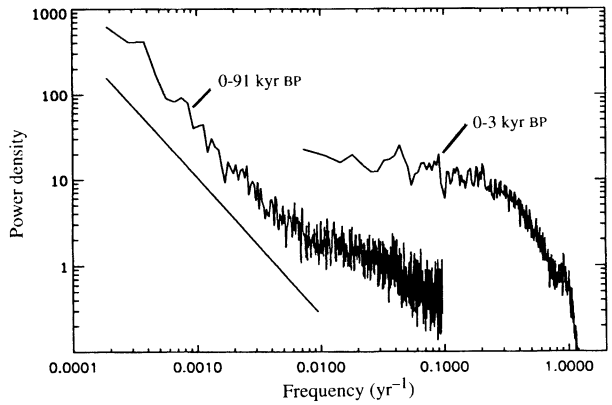

FIG. 2 Power density spectra as a function of frequency for the $\delta^{18}O$ record covering 0–91 kyr BP with a temporal resolution of 10 yr at 91 yr BP (17,496 points). The rightmost, Holocene, spectrum covers 0–3 kyr BP, with a temporal resolution of approximately one month (26,244 points). The spectra have been calculated from the temporal signals using a sliding window. The spectrum has a slope of ~ -1.6 for timescales larger than 100–200 yr, indicated by the line. For timescales smaller than 100–200 yr the spectrum is white until timescales of 5–10 yr. For the Holocene spectrum the annual peak is observed. We see no signs of significant peaks, except for the annual, above the noise level of continuous background in the spectrum. We have used sliding windows of different sizes to look for peaks, but we do not expect an oscillatory behaviour of the climate system on the timescales smaller than those of the orbital forcing. For the orbital periods the record is not long enough for a proper spectral analysis. There are other techniques like singular spectrum analysis (SSA) and the multi-taper method (MTM) designed to extract small peaks from the continuous background, but one must be vary careful when applying these techniques, as they tend to separate realizations of processes with a continuous power spectrum into peaks where the significance tests are rather doubtful, and depend on which null hypothesis is assumed.

ture as represented by the $\delta^{18}O$ itself. Figure 1*d* shows the 10-kyr low-pass of $\delta^{18}O$ (Fig. 1*a*), and Fig. 1*e* shows the 10-kyr low-pass of the absolute value of the high-pass (Fig. 1*c*). The $\delta^{18}O$ signal is a proxy for the local temperature; the relation between the two quantities is that in a cold climate, storm tracks move southwards and the transport route for the precipitation is longer increasing the depletion of ^{18}O. Thus we interpret the increased variance as a direct result of a more stormy—or turbulent—state of the atmospheric flow during the Last Glacial Maximum (LGM).

As an independent measure of the atmospheric and climatic variability we have analysed the probability density functions (PDFs) of the high-pass signal which, in contrast to the low-pass signal, is stationary. The power spectrum of a signal contains information on the second moments and the correlation structure of the signal, whereas the PDFs contains information on all moments but no information on the temporal correlation structure.

A characteristic of the state of turbulent atmospheric flow is the intermittency or occurrence of extreme values in the temperature field as represented through the PDFs[12]. In present-day temperature records, gaussian PDFs are found when subtracting the annual and diurnal cycles. Accordingly, we have analysed the ice-core record for the past 3 kyr, with a temporal resolution of approximately one month (26,244 points), referred to as the Holocene signal in the following. This is compared with the signal covering 14.4–29 kyr BP with a temporal resolution of $\sim$3.7 yr (3,888 points), referred to as the LGM signal in the following. The Holocene signal has a white-noise power spectrum down to 5–10 yr (Fig. 2) where it bends off. This is in agreement with spectra obtained from meteorological data[13,14]. Note the annual cycle in the spectrum. In order to subtract the low-frequency variability, related to non-atmospheric components of the climate system, we examine the high-pass filtered signal, and examine the PDF as a function of the high-pass cutoff frequency. The high-pass signal is normalized with the running variance in a window of 500 data points. The PDF are fitted to Laplace-type distributions[15] of the form $\phi(x) = 1/(2^{1+1/\beta}\Gamma(1+1/\beta)\sigma)\exp(-|x/\sigma|^{\beta}/2)$, which for $\beta = 2$ is the normal distribution and for $\beta = 1$ is the Laplace distribution, Γ is the gamma-function and σ is related to the variance by $\mathrm{var}(x) = \sigma^2 2^{2/\beta}\Gamma(3/\beta)/\Gamma(1/\beta)$. Figure 3*a* shows the normalized 30-yr high-pass for the Holocene signal, Fig. 3*b* shows the cumulated distribution on a normal probability scale, and Fig. 3*c* shows the fitted PDF. This signal is very close to being gaussian. Figure 3*d*, *e* and *f* shows the same for the normalized 30-yr high-pass of the LGM signal. In this case there is a significant deviation from a gaussian distribution. The kurtosis, the normalized fourth-order moment—a measure of the distributions deviation from being gaussian—and the best-fit $\beta = \beta(\kappa)$, signifying the Laplace-type distribution parameter, are shown in Fig. 4 as a function of the high-pass cutoff frequency. Triangles represent Holocene data, and diamonds LGM data; the error bars represent the 95% confidence level[16]. Again the present Holocene climate shows a gaussian distribution (kurtosis = 3, $\beta = 2$) for all timescales, whereas the LGM signal becomes more intermittent for the faster timescales.

Owing to the presence of the ice-sheets and a substantially colder northern ocean[17] in the glacial period, larger thermal gradients between Equator and the glaciers are expected than in the present climate. This would cause a more energetic and turbulent atmosphere in the glacial climate. In the glacial period the distribution of the flat part of the power density spectrum, corresponding to timescales shorter than 100–200 yr, is not trivially gaussian. We believe that the increased variance and—independently—the observed PDFs in the glacial period are observations

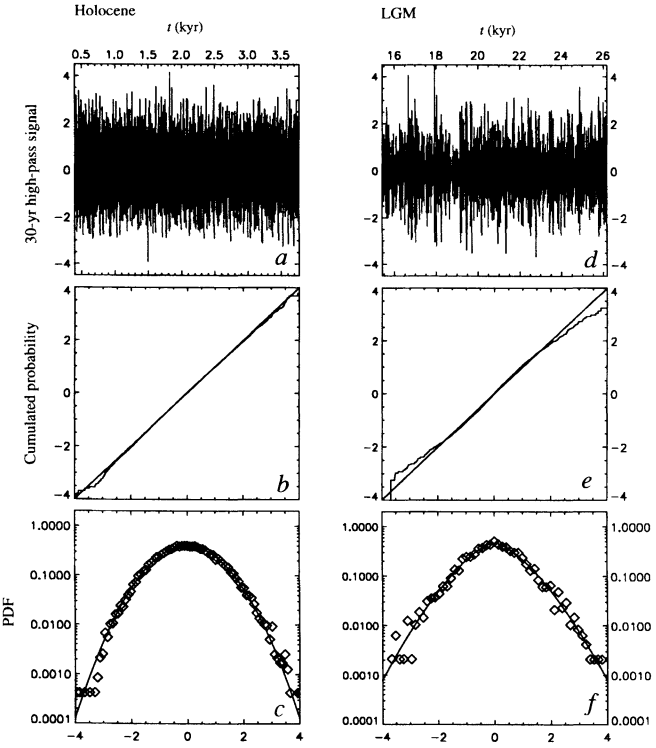

FIG. 3 *a*, The 30-yr high-pass filtered Holocene signal, covering 0–3 kyr BP (26,244 points). The signal is normalized with the variance in a 500-point running window; *b* the cumulated probability on a normal probability scale. The straight line corresponds to the gaussian distribution; *c*, the PDF, which is gaussian. *d*–*f*, As *a*–*c*, but for the LGM signal, covering 14.4–29 kyr BP (3,888 points). The signal is intermittent.

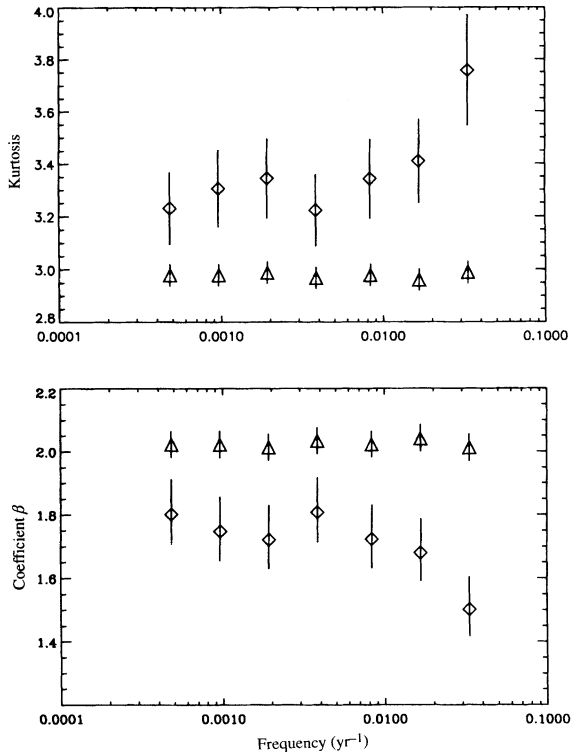

FIG. 4 Top, the kurtosis, $\kappa \equiv E(x^4)/E(x^2)^2$, as a function of the high-pass cutoff frequency. The kurtosis is 3 for the gaussian distribution and 6 for the laplacian distribution. Bottom, the best-fit parameter β (see text) as a function of the high-pass cutoff. For $\beta = 2$ the distribution is gaussian; for $\beta = 1$ it is laplacian. Triangles, Holocene; diamonds, LGM. The error bars are the 95% confidence levels. The Holocene signal is gaussian distributed for all cutoffs, whereas the LGM signal becomes more intermittent when subtracting the longer timescales.

of this more turbulent state of the atmospheric flow reflected in the $\delta^{18}O$ signal in Greenland. This is a direct observation of changes in the atmospheric circulation from palaeoclimate records for the LGM. It supports the indications of circulation changes in glacial climate inferred from correlations between snow accumulation and $\delta^{18}O$ correlations (ref. 18). □

Received 3 April 1995; accepted 24 January 1996.

1. Dansgaard, W. *et al. Nature* **264,** 218–220 (1993).
2. GRIP members *Nature* **364,** 203–207 (1993).
3. Bond, G. *et al. Nature* **365,** 143–147 (1993).
4. Bond, G. C. & Lotti, R. *Science* **267,** 1005–1010 (1995).
5. Fronval, T., Jansen, E., Bloemendal, J. & Johnsen, S. *Nature* **374,** 443–446 (1995).
6. Manabe, S. & Broccoli, A. J. *J. Geophys Res.* **90,** 2167–2190 (1985).
7. Kutzbach, J. E. & Wright, H. E. *Quat. Sci. Rev.* **4,** 147–187 (1985).
8. Rind, D. *J. Geophys Res.* **92,** 4241–4281 (1987).
9. Valdes, P. & Hall, (eds Duplessy, J.-C. & Spyridakis, M.-T.) (NATO ASI ser. 22, Springer, Berlin, 1994).
10. Dahl-Jensen, D. *et al.* (ed. Peltier, W. R.) 517–532 (NATO ASI ser. I 12, Springer, Berlin, 1993).
11. Hasselman, K. *Tellus* **28,** 473–485 (1976).
12. Wu, X. & Libchaber, A. *Phys. Rev.* A**40** 6421–6430 (1989).
13. Willebrand, J. *J. phys. Oceanogr.* **8,** 1080–1094 (1978).
14. Chave, A. D., Luther, D. S. & Filloux, J. H. *J. geophys. Res.* **96,** 18361–18379 (1991).
15. Johnson, N. L. & Kotz, S. *Distributions in Statistics: Continuous Univariate distributions II* (Wiley, New York, 1970).
16. Kendall, M. *et al. Kendall's Advanced Theory of Statistics* (Griffin, London, 1987).
17. Martinson, D. G. *et al. Quat. Res.* **27,** 1–29 (1987).
18. Kapsner, W. R., Alley, R. B., Shuman, C. A., Anandakrishnan, S. & Grootes, P. M. *Nature* **373,** 52–54 (1995).
19. Johnsen, S. J., Dansgaard, W. & White, J. W. C. *Tellus* **B41,** 452–468 (1992).

ACKNOWLEDGEMENTS. We thank J.-P. Steffensen, O. Ditlevsen and P. Dimon for discussions. The Greenland Ice-core Project (GRIP) is a European Science Foundation programme with eight nations collaborating in ice-core drilling. P.D.D. thanks the Carlsberg Foundation for funding.

Correlated progression and the origin of turtles

Michael S. Y. Lee

Zoology Building A08, School of Biological Sciences, University of Sydney, New South Wales 2006, Australia

TURTLES exhibit some of the most extreme postcranial modifications found in vertebrates. The dorsal vertebrae and ribs have fused with dermal armour, forming a totally rigid box-like trunk region[1,2] Our understanding of chelonian origins has been restricted by a paucity of information on intermediate forms[3,4], however, and it is often assumed that they must have evolved saltationally[5]. It has been suggested that pareiasaurs, a group of large herbivorous anapsid reptiles, are the sister-group of turtles[6]. Here I show that certain pareiasaurs—dwarf, heavily armoured forms such a *Nanoparia*—approach the chelonian morphology even more closely than previously thought. Evolutionary trends within pareiasaurs, such as the elaboration of the dermal armour, shortening and stiffening of the presacral region, and increased reliance on limb-driven as opposed to axial-driven locomotion, suggest that the rigid armoured body of turtles evolved gradually, through 'correlated progression'[7].

A consensus has recently been reached that turtles are part of a radiation of primitive reptiles known as 'parareptiles'[8,9], although there is still debate over which 'parareptiles' are closest to turtles: procolophonoids[8] or pareiasaurs[9]. A comprehensive phylogenetic analysis of basal amniotes was therefore undertaken in order to resolve the external relationships of turtles[10]. Ingroup taxa included nycteroleterids, nyctiphruretids, procolophonids, *Barasaurus*, *Owenetta*, lanthanosuchids, *Sclerosaurus*, 'pareiasaurs' and turtles. Because evidence for the monophyly of the Pareiasauridae was weak, each species of pareiasaur was treated as a separate terminal taxon. Previous studies[8,9] had treated pareiasaurs as a single discrete terminal taxon. All valid characters employed in previous analyses were included, although many new informative characters (mostly postcranial) were identified. The two nearest outgroups (millerettids and 'eureptiles'[8]) were used to polarize characters. The data were analysed using the branch and bound algorithm of PAUP 3.1.1.

The results confirm that pareiasaurs are the nearest relatives of turtles, although the exact nature of this relationship remains equivocal. In the most parsimonious tree (221 steps, c.i. = 0.77, r.i. = 0.92), pareiasaurs are ancestral to (that is, paraphyletic with respect to) turtles (Fig. 1). Large (2.5m long, excluding tail) heavily ossified pareiasaurs such as *Bradysaurus baini* and *Embrithosaurus schwarzi* are quite distantly related to turtles. Slightly closer to turtles is the smaller (2 m) and more lightly built *Deltavjatia vjatkensis*. Closer still is a clade of pareiasaurs with prominent cranial bosses: *Scutosaurus karpinskii*, *Elginia mirabilis*, *Pareiasuchus nasicornis*, *P. peringueyi* and *Pareiasaurus serridens*. The nearest relatives of turtles are the late, dwarf (<1 m long) heavily armoured forms *Anthodon serrarius* and *Nanoparia pricei*. However, there is conflicting evidence suggesting that pareissaurs are the monophyletic sister group of turtles: the shortest tree consistent with this hypothesis is only 248 steps.

The evolution of the dermal armour within pareiasaurs sheds light on how the distinct carapace of turtles might have evolved. The most primitive arrangement of dermal armour is exhibited by the early, basal pareiasaurs *Bradysaurus*, *Embrithosaurus* and *Deltavjatia* (Fig. 1). Here, the osteoderms are small isolated discs restricted to the dorsal midline, immediately above the vertebral column. The flanks, and much of the dorsum, were unarmoured. Dermal armour in pareiasaurs therefore initially did not serve a protective function. Rather, this arrangement of osteoderms has been shown to have a postural role, providing extra areas of insertion for the axial musculature[11]. It is not